Rakenteiden Mekaniikka (Journal of Structural Mechanics)
Vol. 49, No 2, 2016, pp. 36 – 51
rmseura.tkk.fi/rmlehti/

VERTAISARVIOITU
KOLLEGIALT GRANSKAD
PEER-REVIEWED
www.tsv.fi/tunnus

A shell facet model for preliminary design of cylindrical composite structures

Harri Katajisto, Petri Kere[1], and Mikko Lyly

Summary. The laminated composite lay-up design typically involves trade-offs between material selection, thickness of the layer, orientation of the layers, and the stacking sequence. Finding the right structural concept early in the design process leaves resources for the detailed design. Many structural members made of laminated composite materials have the form of thin walled cylindrical shells that are prone to buckling. Thus it is desirable to find structural designs that satisfy global requirements for structural stability early in the design phases. In this work, thin-walled cylindrical composite shells under different loading conditions have been studied for structural stability. The simulation is performed with a shell facet model implemented in the ESAComp software. Preliminary design tools for structural stability of thin-walled cylindrical composite shells are demonstrated and discussed.

Key words: cylindrical shells, laminated composites, shell facet model, stability, finite element methods

Received 3 February 2016. Accepted 1 June 2016. Published online 9 December 2016

In memory of Professor Juhani Koski

Introduction

Fiber-reinforced polymer composites are usually thin-walled laminated shell structures that are prone to buckling. The laminated composite lay-up design typically involves trade-offs between material selection, thickness of the layer, orientation of the layers, and the stacking sequence [1, 23]. Fast and reliable computational methods for stability analysis of laminated composite shell structures are required in the preliminary design phase.

Low buckling loads and geometrical imperfections are closely related for thin-walled cylinders [3, 17, 18, 20]. Already at small imperfection amplitudes the actual buckling load can be well below the result obtained for an ideal structure with linear buckling analysis. By definition, a geometrical imperfection is a deviation from the perfect cylindrical geometry. Geometrical imperfections have been demonstrated to have clearly the highest influence on the buckling load when compared to, for example, the effect of thickness variations, stress variations, and boundary stiffness. The real imperfections are often unknown, but in the design process the influence of the imperfections has to be taken into

[1]Corresponding author. petri.kere@kone.com

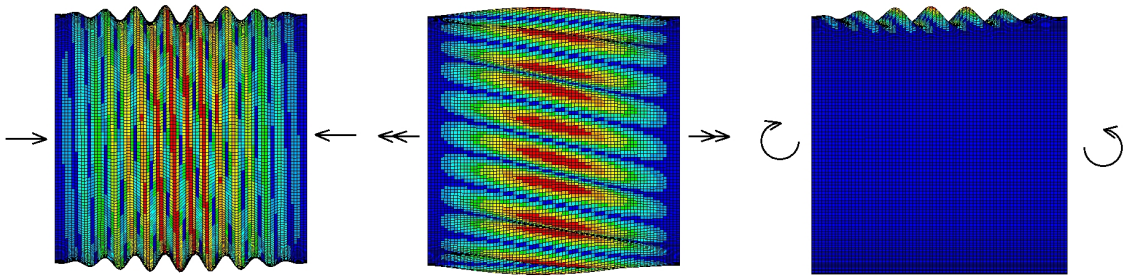

Figure 1. Cylinder load cases – axial, torque, bending.

account properly to achieve a safe structure. Design guidelines, such as NASA SP-8007 [4], do not require knowledge about the pattern or even amplitude of the imperfections. Instead, very conservative knock-down factors are used.

Measuring the real imperfections and implementing them into the numerical analysis have been traditionally very costly, but result in less conservative design loads. Realistic geometrical imperfections in a numerical analysis are such that they describe the existing pre-buckling shape and size as good as possible. This approach assumes that specific manufacturing processes statistically result in basically the same imperfections. It has been assumed that the eigenform affine patters are the worst imperfections. Later, axisymmetric imperfections were believed to show the worst behavior.

Stimulating imperfections is another approach where a local imperfection is generated to the geometry. The Single Perturbation Load Approach (SPLA) belongs to this class and it has been widely studied in the ongoing DESICOS project [13, 15, 18, 20]. Hühne [17, 18] showed by numerical and experimental investigations that the collapse of cylindrical shells always starts with a single buckle.

In the preliminary design often 3D model can be idealized with simplified geometry. Focus is in the material selection and laminate lay-up design. Numerous iterations are needed and therefore, model creation needs to be easy, computation time short and results need to be reliable. The presented shell facet model as such suits also in the detailed design phase, but typically that design phase involves, at least partly, solid modeling to consider discontinuities.

In this work, thin-walled cylindrical shells with radius-to-thickness ratio of 160-500 under different loading conditions as shown in Figure 1 have been studied for structural stability. The simulation is performed with a shell facet model implemented in the ESAComp software [1] The shell facet model was implemented with the Elmer open-source Finite Element Method (FEM) solver [2, 19, 21] developed by CSC - IT Center for Science (CSC) in collaboration with Finnish universities, research laboratories, and industry.

ESAComp development started in 1992 at Helsinki University of Technology (now known as Aalto University) as a project initiated by the European Space Agency (ESA). In 2000 Componeering, a Helsinki based company founded by the original project team, took over the development. ESAComp is a proprietary licensed software owned by Componeering. ELMER technology has been integrated in ESAComp for the realization of the FE analysis capability with an agreement between Componeering and CSC.

The ESAComp software provides a user-friendly approach to introduce geometrical imperfections into the geometry. The shape of the imperfection can be generated with a linear buckling analysis and scaled by a user-defined amplitude. For cylindrical shells

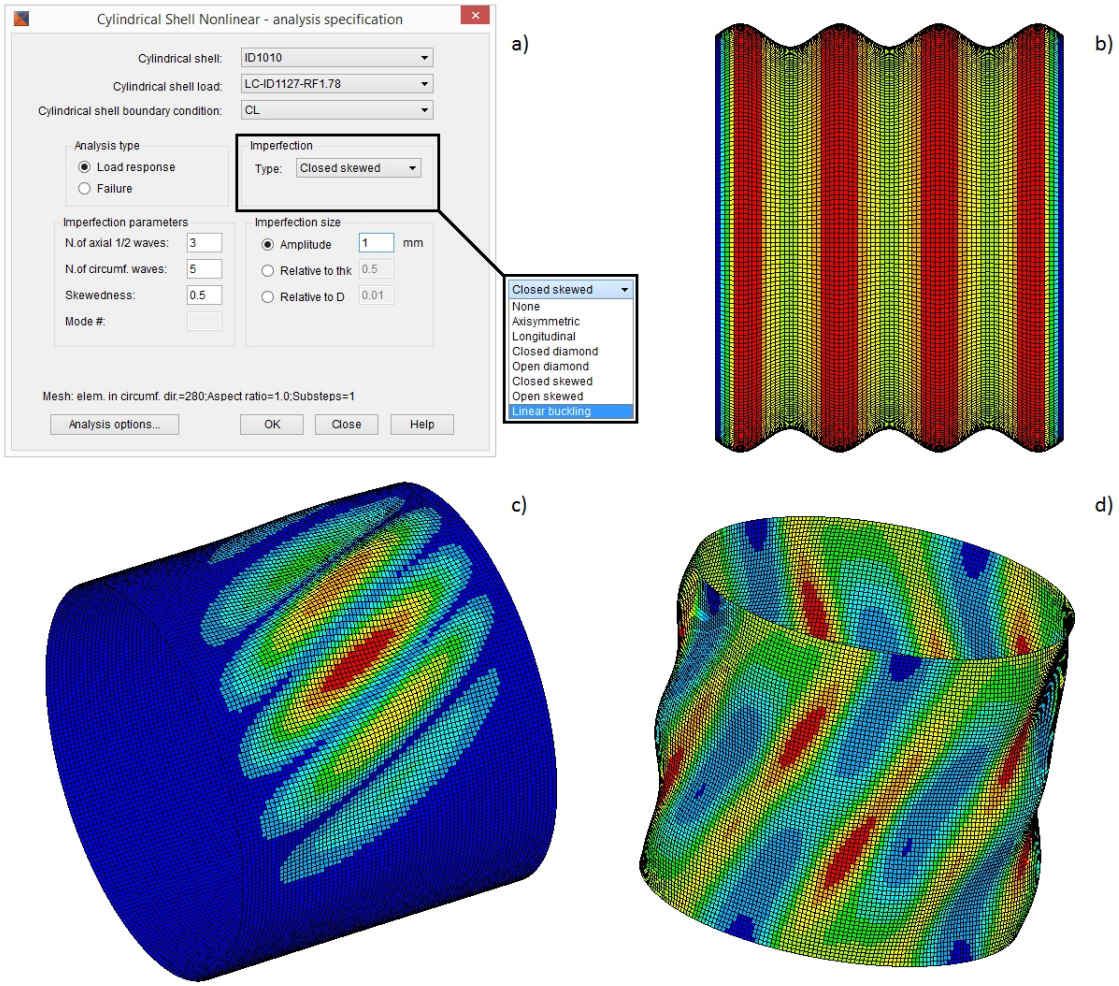

Figure 2. a) The ESAComp [1] specification dialog for cylinder analysis; b) an axisymmetric imperfection with seven half-waves; c) the first buckling mode shape according to the linear buckling analysis; d) a closed skewed imperfection - the end cross-sections of the cylinder have a perfect round shape. There are three axial half-waves and five circumferential waves in the structure. The skewedness parameter has been set to 0.5. The amplitude of the imperfection has been extended for visualization.

the distorted shape can be based on analytical formulas as well. Various possibilities are illustrated in Figure 2. In ESAComp, Reissner-Mindlin-von Kármán type shell facet model [19, 21] is used for geometrically nonlinear analyses. Tools implemented in ESAComp are used to study the imperfection sensitivity through the alternation of the shape and amplitude of the imperfection.

Reissner-Mindlin-von Kármán type shell facet model

The plate bending problem is formulated for a thin or moderately thick laminated composite plate which in its undeformed configuration occupies the region $\Omega \times (-t/2, t/2)$, where $\Omega \subset \mathbb{R}^2$ is the midsurface and $t > 0$ is the laminate thickness. The kinematical unknowns in the model are transverse deflection w, in-plane displacement $u = (u_x, u_y)$, rotation of the shell reference surface $\beta = (\beta_x, \beta_y)$, and drilling rotation ω. The plate is subjected to the in-plane load $f = (f_x, f_y)$ and the transverse pressure g at its reference plane.

Let us note that our model is actually a numerical "shell facet model" since we are in fact considering one element in the mesh. As far as we know, there is no mathematical analysis guaranteeing the consistency of this very classical engineering approach, but it seems to work fine in practice.

We will use standard notation of tensor calculus. Dyadic and index notation with summation convention over repeated indices are used in parallel. Latin indices take their values in the set $\{1, 2, 3\}$ and Greek indices in the set $\{1, 2\}$.

Constitutive relation for a single layer

Let us denote by e_i and $\bar{e}_j$ the cartesian basis vectors for the so called 123-coordinate system of a single ply, and for the xyz-system of material coordinates common to all plies, respectively. In the material coordinate system, i.e., the laminate coordinate system, the layer system has been rotated by a positive counter clockwise angle θ about the z-axis. Hence, we define the transformation matrix between the two coordinate systems as $T = T_{ij} = e_i \cdot \bar{e}_j$, or

$$T = \begin{bmatrix} \cos\theta & \sin\theta & 0 \\ -\sin\theta & \cos\theta & 0 \\ 0 & 0 & 1 \end{bmatrix} \tag{1}$$

For linear orthotropic materials, a plane stress state is assumed and the constitutive relation for each ply has the form

$$\sigma = Q : \epsilon \tag{2}$$

where $\sigma = \sigma_{ij} = \sigma_{ji}$ is the second order stress tensor, $\epsilon = \epsilon_{ij} = \epsilon_{ji}$ is the strain tensor, and $Q = Q_{ijkl} = Q_{jikl} = Q_{ijlk} = Q_{klij}$ is the fourth order tensor of elastic stiffness coefficients. In the laminate coordinate system the constitutive equation is written as

$$\bar{\sigma} = \bar{Q} : \bar{\epsilon} \tag{3}$$

where $\bar{\sigma}_{ij} = T_{ip}T_{jq}\sigma_{pq}$ is the laminate stress, $\bar{\epsilon}_{ij} = T_{ip}T_{jq}\epsilon_{pq}$ is the laminate strain, and $\bar{Q}_{ijkl} = T_{ip}T_{jq}T_{kr}T_{ls}Q_{pqrs}$ is the tensor of stiffness coefficients in the laminate coordinate system.

The six independent non-zero components of Q are computed using the orthotropic material engineering constants $E_1, E_2, \nu_{12}, \nu_{21} = \nu_{12}E_2/E_1, G_{12}, G_{23}$, and G_{31} [16] as

$$\begin{gathered} Q_{1111} = E_1/(1-\nu_{12}\nu_{21}),\ Q_{2222} = E_2/(1-\nu_{12}\nu_{21}), \\ Q_{1122} = \nu_{12}E_2/(1-\nu_{12}\nu_{21}), \\ Q_{1212} = G_{12},\ Q_{2323} = G_{23},\ Q_{3131} = G_{31} \end{gathered} \tag{4}$$

Kinematic relations for a laminate

The kinematic relations for a laminate are considered in the xyz-coordinate system. For notational simplicity, laminate stresses and strains in the xyz-coordinate system are in the following denoted without bar symbol.

Using the classical kinematic assumptions of Reissner, Mindlin, and von Kármán the laminate strain is obtained from

$$\epsilon = \varepsilon(u) + \varphi(u, w) - z\varepsilon(\beta) \tag{5}$$

and

$$\epsilon_{3\alpha} = \gamma_\alpha(w, \beta), \quad \epsilon_{33} = 0 \tag{6}$$

where $z := x_3$, ε is the linear strain tensor, φ is the nonlinear membrane strain tensor, and γ the transverse shear strain vector, viz.

$$\varepsilon(u) = \frac{1}{2}(\nabla u + \nabla u^T) \tag{7}$$

$$\varphi(u, w) = \frac{1}{2}(\nabla u_x \otimes \nabla u_x + \nabla u_y \otimes \nabla u_y + \nabla w \otimes \nabla w) \tag{8}$$

$$\gamma(w, \beta) = \nabla w - \beta \tag{9}$$

Let us note that the original von Kármán strains [3] do not have the quadratic in-plane displacement gradients in the membrane tensor φ. The quadratic in-plane displacement gradients are considered in the model for the sake of completness and they are not expected to enhance the accuracy of the original model significantly.

Constitutive relations for a laminate

In plane-stress state, the laminate membrane stress resultants N (forces per unit length) and bending moment resultants M (moments per unit length) are obtained by integration of the stress resultants of all layers $z_{k-1} < z < z_k$, $k = 1, \ldots, n$, over the thickness of the laminate as

$$N = \int_{-t/2}^{t/2} \sigma dz = \sum_k \int_{z_{k-1}}^{z_k} \sigma dz \tag{10}$$

$$M = \int_{-t/2}^{t/2} \sigma z dz = \sum_k \int_{z_{k-1}}^{z_k} \sigma z dz \tag{11}$$

Furthermore, the resultant transvere shear forces S are obtained from

$$S = \int_{-t/2}^{t/2} \sigma_{3\alpha} dz = \sum_k \int_{z_{k-1}}^{z_k} \sigma_{3\alpha} dz \tag{12}$$

Using the constitutive equation and the kinematic relations of Reissner, Mindlin, and von Kármán we get the following constitutive relations for the laminate

$$N(u, w, \beta) = A : [\varepsilon(u) + \varphi(u, w)] + B : \varepsilon(\beta) \tag{13}$$

$$M(u, w, \beta) = B : [\varepsilon(u) + \varphi(u, w)] + D : \varepsilon(\beta) \tag{14}$$

$$S(w, \beta) = A^\star \cdot \gamma(w, \beta) \tag{15}$$

The tensors A, B, and D are defined according to the Classical Lamination Theory (CLT) [16] as

$$A = \sum_k \int_{z_{k-1}}^{z_k} \bar{Q}\ dz = \sum_k (z_k - z_{k-1}) \bar{Q}^{(k)} \tag{16}$$

$$B = \sum_k \int_{z_{k-1}}^{z_k} \bar{Q} z\ dz = \frac{1}{2} \sum_k (z_k^2 - z_{k-1}^2) \bar{Q}^{(k)} \tag{17}$$

$$D = \sum_k \int_{z_{k-1}}^{z_k} \bar{Q} z^2\ dz = \frac{1}{3} \sum_k (z_k^3 - z_{k-1}^3) \bar{Q}^{(k)} \tag{18}$$

where $\bar{Q}^{(k)}$ defines the constitutive relation for linear orthotropic materials in plane stress state for layer k in the laminate coordinate system.

The tensor for transverse shear stiffness $A^\star$ can be defined according to the CLT [16] as

$$A^\star_{ij} = \sum_k \int_{z_{k-1}}^{z_k} \bar{Q}_{3i3j}\ dz = \sum_k (z_k - z_{k-1}) \bar{Q}^{(k)}_{3i3j} \tag{19}$$

In ESAComp [1], the computation of the out-of-plane shear stress distribution and stiffness is based on the theory developed at German Aerospace Center (DLR) [12]. First Order Shear Deformation Theory (FSDT), i.e., the out-of-plane shear deformation is considered as an extension to the CLT plane stress assumption in ESAComp.

The shell facet model

The functions u, w, β, ω are determined from the condition that they minimize the potential energy of the plate. The energy is defined as

$$\begin{aligned}
\Pi(u,w,\beta,\omega) &= \frac{1}{2}\int_\Omega N(u,w,\beta) : [\varepsilon(u) + \varphi(u,w)]\ d\Omega \\
&+\frac{1}{2}\int_\Omega M(u,w,\beta) : \varepsilon(\beta)\ d\Omega + \frac{1}{2}\int_\Omega S(w,\beta)\cdot\gamma(w,\beta)\ d\Omega \\
&+C\int_\Omega [\omega - rot(u)]^2\ d\Omega - \int_\Omega f\cdot u\ d\Omega - \int_\Omega gw\ d\Omega
\end{aligned} \tag{20}$$

where $C > 0$ is a penalty parameter for imposing the condition $\omega = rot(u)$ (see [7]), and

$$rot(u) = \frac{\partial u_x}{\partial y} - \frac{\partial u_y}{\partial x} \tag{21}$$

Substituting the constitutive equations in Eq. 20, we get

$$\begin{aligned}
\Pi(u,w,\beta,\omega) &= \frac{1}{2}\int_\Omega \varepsilon(u) : A : \varepsilon(u)\ d\Omega + \int_\Omega \varepsilon(u) : B : \varepsilon(\beta)\ d\Omega \\
&+\frac{1}{2}\int_\Omega \varepsilon(\beta) : D : \varepsilon(\beta)\ d\Omega + \frac{1}{2}\int_\Omega \gamma(w,\beta)\cdot A^\star\cdot\gamma(w,\beta)\ d\Omega \\
&+C\int_\Omega [\omega - rot(u)]^2\ d\Omega + \frac{1}{2}\int_\Omega \varphi(u,w) : A : \varphi(u,w)\ d\Omega \\
&+\int_\Omega \varepsilon(u) : A : \varphi(u,w)\ d\Omega + \int_\Omega \varepsilon(\beta) : B : \varphi(u,w)\ d\Omega - \int_\Omega f\cdot u\ d\Omega - \int_\Omega gw\ d\Omega
\end{aligned} \tag{22}$$

Geometrically nonlinear analysis

To obtain the load-displacement curve and to study the stability behaviour, the nonlinear equations are solved iteratively by Riks' method with Crisfield's elliptical constraint for arc length [5, 6, 9]. The differential equilibrium equations of the minimization problem are obtained using standard variational calculus and integration by parts. The linearized equations are then discretized by the finite element method.

The algorithm is based on the Newton iteration, which follows the principal equilibrium path. The resulting linear system is solved by minimizing the energy, and if there is no minimum, i.e., if there is a negative coefficient matrix, it will terminate. All solutions presented in the paper are obtained for positive definite coefficient matrices. Hence, in

the post-buckling region the algorithm follows the principal equilibrium path with the minimal stiffness.

Let the equilibrium equation be defined as

$$F(q,\lambda) \equiv \lambda P(q) - R(q) = 0 \tag{23}$$

where the unbalanced or residual force is denoted by F, P and R are the external and internal loads, respectively, $q = (u_x, u_y, w, \beta_x, \beta_y, \omega)$ are the nodal displacements of the FE-solution and λ is the load scaling factor serving as a control parameter of the system. In this work, the reference load P is assumed to be independent of q.

Using the arc-length methods for solving the nonlinear equilibrium equations, the load-displacement constraint G is added to the system

$$H(q,\lambda) = \begin{cases} F(q,\lambda) = 0 \\ G(q,\lambda) = 0 \end{cases} \tag{24}$$

Solution of the nonlinear system is obtained by an incremental approach with the elliptical constraint and the algorithm as follows:

1. Given a solution (q_e, λ_e) to Eq. 24, define $G(q,\lambda) = (q-q_e)^T W (q-q_e) + c^2(\lambda - \lambda_e)^2 - s^2$, where W is a positive weighting matrix for the displacements, c is a load scaling parameter, and s is the arc length.

2. Linearize in the intermediate state (q_i, λ_i) as

$$H(q,\lambda) \approx \begin{cases} F(q_i,\lambda_i) + \frac{\partial F}{\partial q}(q_i,\lambda_i)(q-q_i) + \frac{\partial F}{\partial \lambda}(q_i,\lambda_i)(\lambda-\lambda_i) = 0 \\ G(q_i,\lambda_i) + \frac{\partial G}{\partial q}(q_i,\lambda_i)(q-q_i) + \frac{\partial G}{\partial \lambda}(q_i,\lambda_i)(\lambda-\lambda_i) = 0 \end{cases} \tag{25}$$

   or

$$\begin{cases} F(q_i,\lambda_i) + K(q-q_i) + P(\lambda-\lambda_i) = 0 \\ G(q_i,\lambda_i) + 2(q_i-q_e)^T W(q-q_i) + 2c^2(\lambda_i-\lambda_e)(\lambda-\lambda_i) = 0 \end{cases}$$

   where $K = \frac{\partial F}{\partial q}(q_i,\lambda_i)$ is a tangent to the equilibrium path at an equilibrium state.

3. Solve (q,λ) from Eq. 25. If $|H(q,\lambda)| \leq \delta$ goto Step 4 else set $(q_i,\lambda_i) = (q,\lambda)$ and goto Step 2.

4. Set $(q_e,\lambda_e) = (q,\lambda)$ and goto Step 1.

In ESAComp [1], the load controlled method is applied with $W = 0$ and load scaling parameter $c = 1$.

FE-implementation

In the FE-implementation bilinear stabilized MITC plate elements [8, 10, 14] are used. The shear energy term is modified as

$$\frac{1}{2}\,\frac{t^2}{t^2+\alpha h^2}\int_\Omega \gamma_h(w,\beta)\cdot A^\star \cdot \gamma_h(w,\beta)\; d\Omega \tag{26}$$

where $\alpha > 0$ is a numerical stabilization parameter, h is the mesh parameter, i.e., the largest side length, and γ_h is the reduced shear strain [8, 14].

For the bilinear quadrilateral element used in the simulation, the reduced shear is defined locally such that

$$\gamma_h(w,\beta)_{|K} = \begin{bmatrix} a_K + c_K y \\ b_K + d_K x \end{bmatrix} \tag{27}$$

for every element K. The parameters a_K, b_K, c_K, and d_K are determined from the condition

$$\int_e [\gamma(w,\beta) - \gamma_h(w,\beta)] \cdot \tau \; ds = 0 \tag{28}$$

for every edge e of K. Here τ is the tangent to the edge. In the computation, the in-plane forces N and the bending moments M are obtained consistently from the constitutive equations. Shear forces are computed from

$$S(w,\beta) = \frac{t^2}{t^2 + \alpha h^2} A^\star \cdot \gamma_h(w,\beta) \tag{29}$$

The computation of the out-of-plane shear stress distribution and stiffness in ESAComp is based on the theory developed at German Aerospace Center (DLR) [12]. In this work, shear stabilization parameter α and drilling stabilization parameter C have fixed values of 0.2. Those can be manually adjusted from model template files of ESAComp.

Examples

Selection of element mesh density

Thin-walled Carbon-Fiber-Reinforced Polymer (CFRP) cylindrical shells with radius-to-thick-ness ratio R/t of 160-500 under different loading conditions shown in Figure 1 were studied for structural stability. Based on this study, guidelines for the selection of the element mesh density were set.

A set of problems presented in Table 1 was solved with ESAComp using different mesh densities. The load types considered were axial compression, torsion, and bending. The number of elements in the hoop direction N_h was set to vary from 40 to 240 while the element aspect ratio was set to one.

Convergence studies were made and the results are presented for the axial load in Figure 3 on top. Respectively, results for the torsion and bending cases are shown on bottom of Figure 3. The reserve factor against buckling RF indicated on the vertical axis has been normalized against the value obtained with 240 elements in the hoop direction.

A short summary for the problems are presented in Table 1. The deviation δ indicates the difference between the ESAComp results with respect to the reference results at the converged state using the linear buckling analysis.

As an outcome of this study it can be concluded that in axial load dominated buckling 160 elements are needed in the hoop direction to achieve reasonable accuracy, i.e., the deviation from the converged result is less than 10 percent. For torsion and bending dominated buckling, 120 elements is a sufficient number to guarantee the same accuracy since in these problems buckling wave lengths are longer. It should be noted that in this study cylinder diameter-to-length ratio D/L was equal or close to one.

Nonlinear analysis of a cylindrical structure with imperfection sensitivity study

A thin-walled axially compressed CFRP cylinder was studied using the large deformation analysis with Reissner, Mindlin, and von Kármán type shell facet models. Different

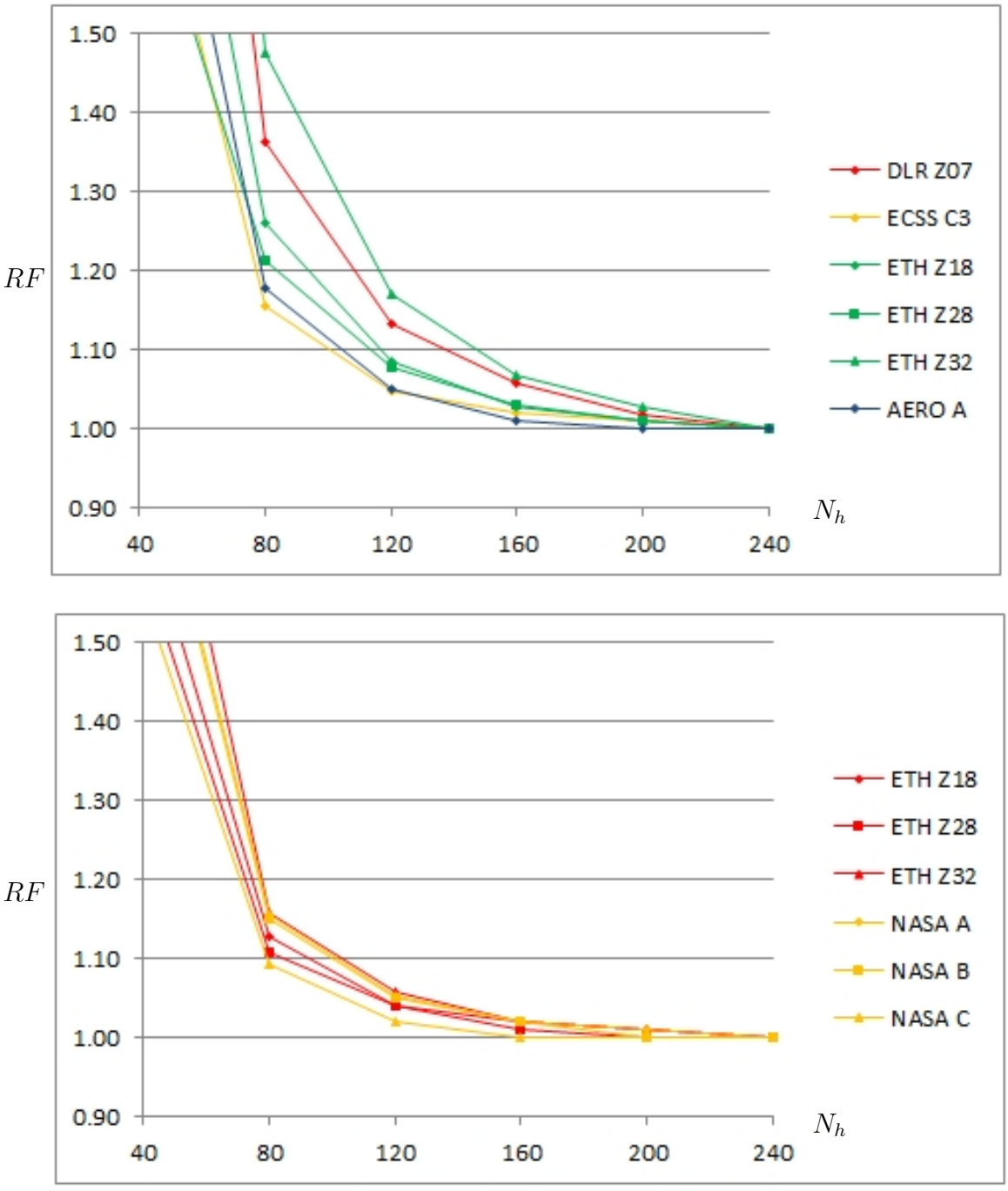

Figure 3. A mesh convergence study. Reserve Factor RF against buckling calculated for various cylinder configurations (see Table 1) using different mesh densities. The mesh density is considered with the number of elements in the hoop direction N_h. N_h was set to vary from 40 to 240 while the element aspect ratio was set to one. RF indicated on the vertical axis has been normalized against the value obtained with 240 elements in the hoop direction. The graph illustrates how coarser element meshes give optimistic predictions for the load carrying capability in stability.

Table 1. The deviation δ between the results computed with ESAComp [1] with respect to the reference results [11, 13, 15, 18, 20] at the converged state using the linear buckling analysis. Load components axial, torque and bending are illustrated in Figure 1. Geometrical parameters are diameter of the cylinder D, length of the cylinder L, radius of the cylinder R, and thickness of the cylinder t.

Cylinder	Load	D/L	R/t	δ [%]
DLR [18] Z07	axial	1	500	+5
ECSS [20] C3	axial	1.1	100	+3
ETH [15] Z18	axial	1	200	+4
ETH [15] Z18	torque	1	200	+2
ETH [15] Z28	axial	1	200	+3
ETH [15] Z28	torque	1	200	+2
ETH [15] Z32	axial	1	200	+5
ETH [15] Z32	torque	1	200	+2
AERO [13] A	axial	1.3	265	+1
NASA [11] A	bending	1	160	−4
NASA [11] B	bending	1	160	−1
NASA [11] C	bending	1	160	−2

numbers of axial, circumferential and combined imperfection waves were used to represent the initial shape of the structure. Three examples are shown at the bottom of Figure 4. The horizontal axis of the chart corresponds to the number of axial half-waves and the vertical axis to the number of circumferential waves. The amplitude of the imperfection was 0.2 mm, which has been magnified by a factor of 100 for the visualization. The reference application is the Z15 benchmark cylinder used in DESICOS project [13, 15, 18, 20].

The nominal load used in this sensitivity study corresponded to the SPLA design buckling load of 17.99 kN. The results of the sensitivity study are presented in the bubble chart of Figure 4. Color codes from red to blue and bubble sizes from small to large indicate the increasing load factor with respect to the SPLA.

In SPLA a geometrical imperfection is created with a radial perturbation load P. For the reference application the perturbation load P was as small as 3 N. Using the ESAComp panel analysis, which is applicable to semi-cylinders shown in Figure 5, the deformation level with $P = 3$ N was solved. The maximum deformation was slightly over 0.2 mm and therefore, the selected amplitude in the sensitivity study was 0.2 mm. The radial perturbation force generates a local axial half-wave and oscillating circumferential waves. If we assume that there are multiple equally spaced perturbation loads, the initial imperfect shape can be generated with ESAComp, for example, by assuming that there is a single axial half-wave and eight circumferential waves. Generally the study was made with the imperfection amplitude of 0.2 mm. However, a single result was generated with the imperfection amplitude of 2 mm. This is presented in the chart of Figure 5 by the red bubble with a black border.

In ESAComp, the nonlinear equations are solved iteratively by Riks' method with the load-controlled incrementation scheme and Reissner, Mindlin, and von Kármán type shell facet model. The number of sub-steps is defined through the analysis options. The

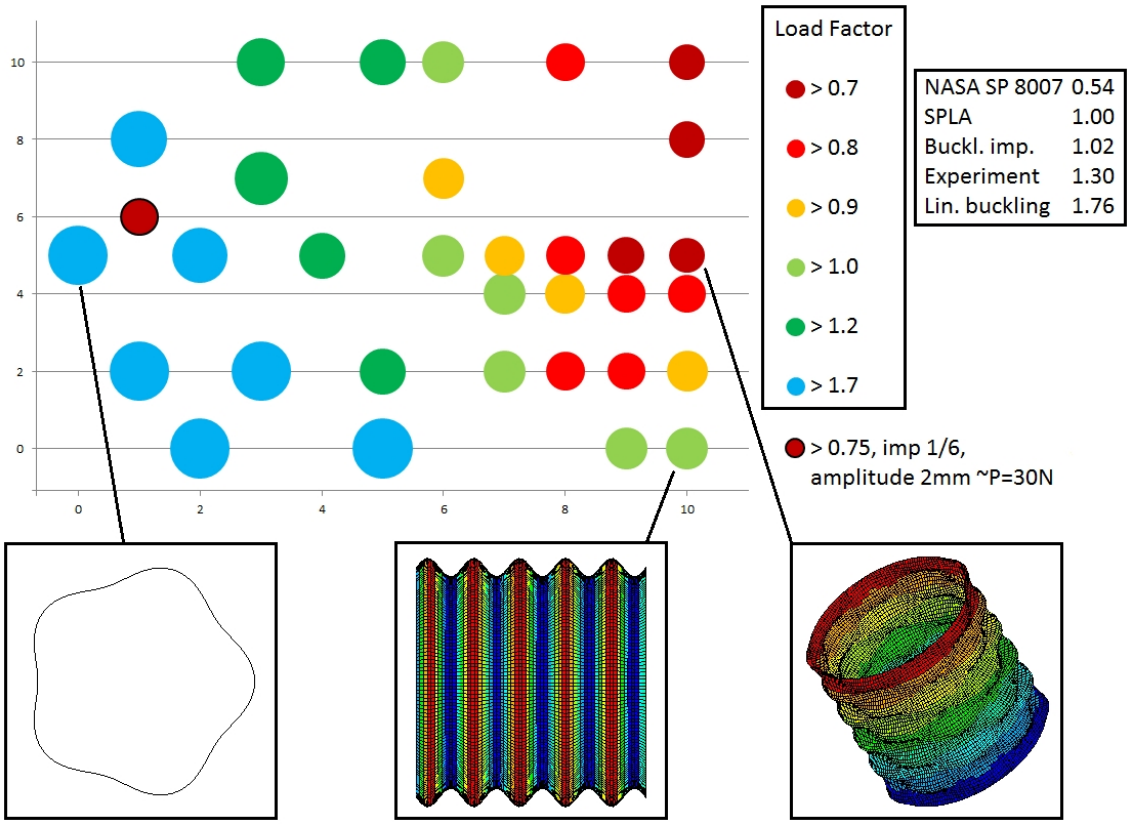

Figure 4. Results of the sensitivity study.

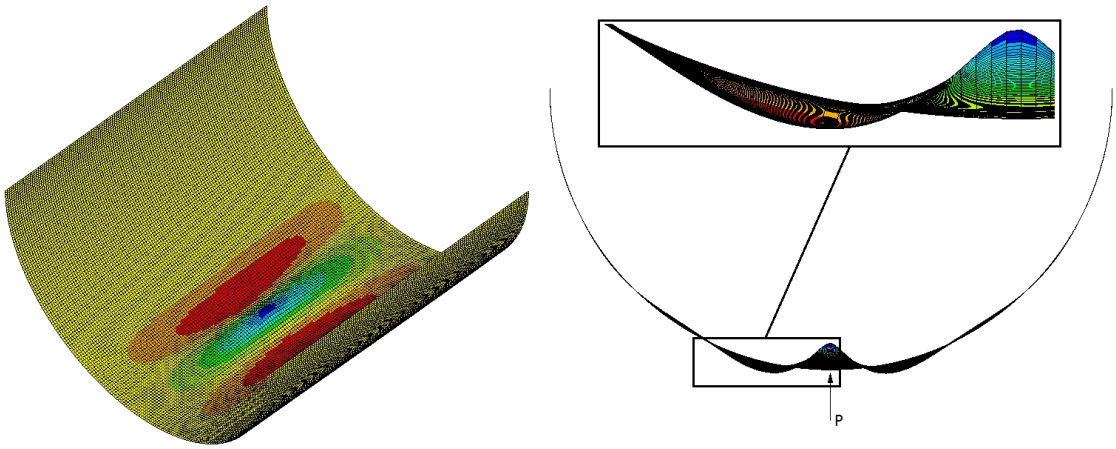

Figure 5. Deformed shape of the semi-cylinder loaded with a single perturbation force P.

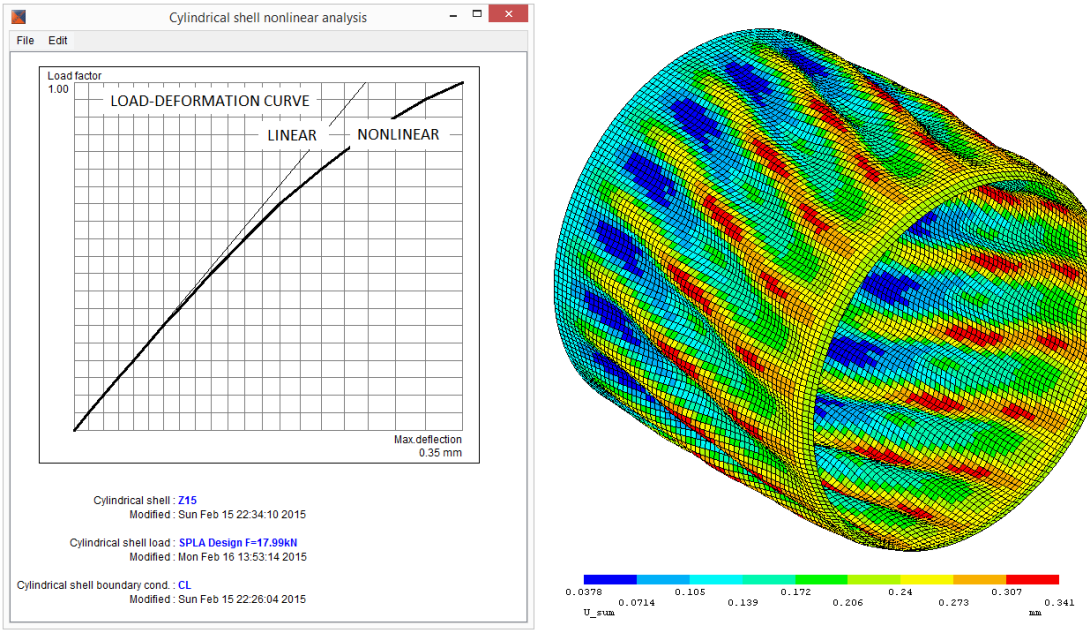

Figure 6. The result tracker (left) and the deformed cylinder (right) for which the initial shape was generated using the linear buckling analysis.

nonlinear analysis of ESAComp provides on-line monitoring. The result tracker indicates how the maximum deflection of the structure develops as a function of the load increment and thus gives a direct indication at which load level the structure starts to behave in a nonlinear manner. The graph in Figure 6 is related to the cylinder for which the initial shape has been obtained from the linear buckling analysis. The presented solution has just converged with the design load. The deformation has been scaled by a factor of 100 for the visualization. A load factor of 1.02 was obtained for this configuration and this is indicated in Figure 4 as "Buckl. imp."

Design-optimization of cylindrical composite structures

Generally optimization aims to the selection of the best, or a set of best suited designs, with respect to one or more objectives and a set of constraints. The design-optimization of cylindrical, layered composite structures for a launcher application is described in detailed in reference [22]. The goal of the optimization was to minimize the weight of the cylinder while meeting the constraints related to the stability and laminate strength. The project was realized by combining ESAComp with a design optimization and process integration software. Sandwich structures may provide the optimum solution in some applications. Also, stiffened structures as shown in Figure 7 are widely used.

Conclusions

A set of problems for CFRP cylindrical shells presented in the literature has been solved using a shell facet model and tools implemented in the ESAComp software for structural stability analysis. In this work, the load types considered were axial compression, torsion, and bending. The number of elements in the hoop direction was set to vary from 40 to 240 while the element aspect ratio was set to one. Convergence studies show that in axial load dominated buckling, 160 elements are needed in the hoop direction to achieve reasonable

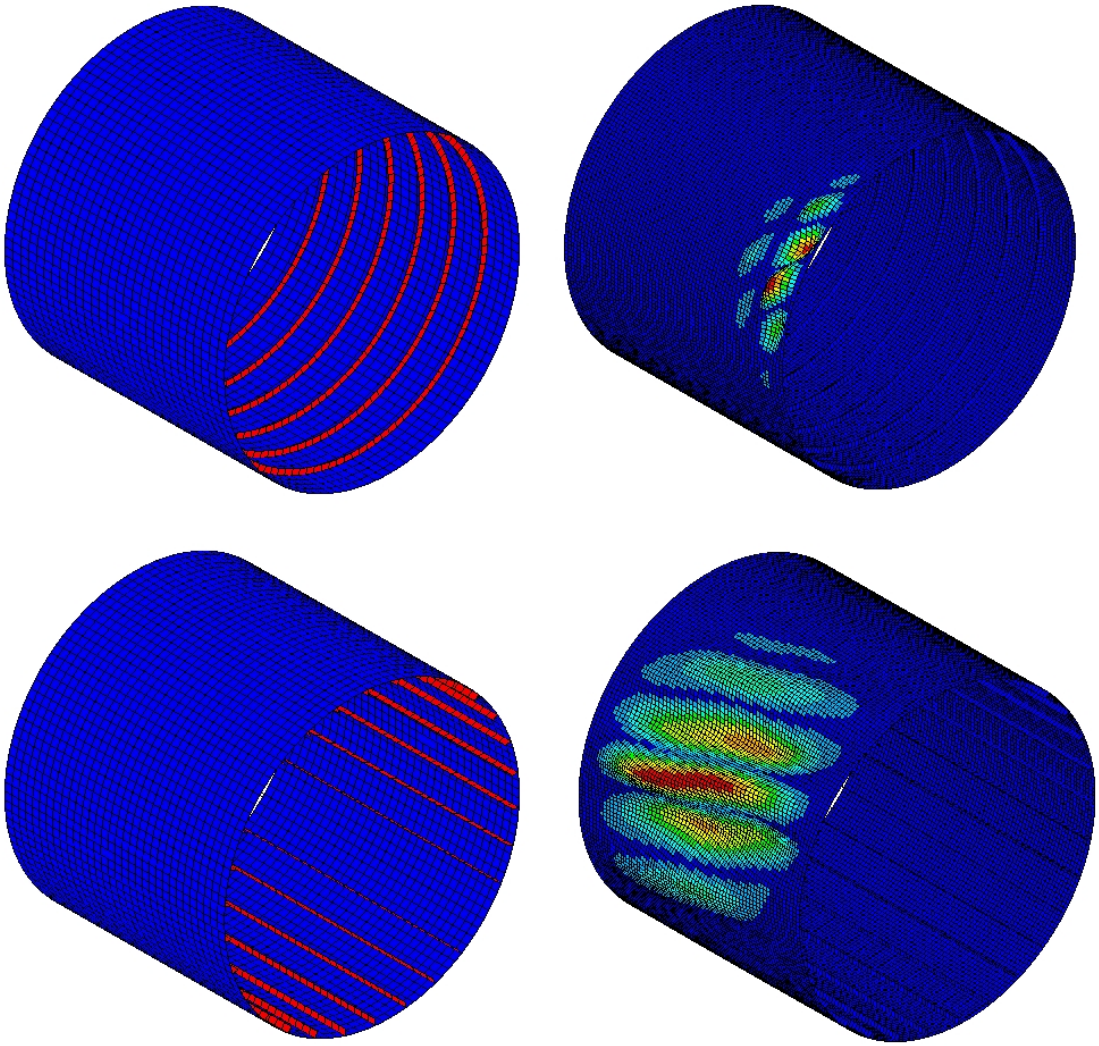

Figure 7. Buckling of the cylinder with ring stiffeners (on top) and with axial stiffeners (on bottom).

accuracy, i.e., the deviation from the converged result is less than 10 per cent. For torsion and bending dominated buckling, 120 elements is a sufficient number to guarantee the same accuracy since in these problems buckling wave lengths are longer. In this study, the cylinder diameter-to-length ratio was equal or close to one.

In ESAComp, the nonlinear equations are solved iteratively by Riks' method with the load-controlled incrementation scheme. The number of sub-steps is defined through the analysis options. The nonlinear analysis of ESAComp provides on-line monitoring. The result tracker indicates how the maximum deflection of the structure develops as a function of the load increment and thus gives a direct indication at which load level the structure starts to behave in a nonlinear manner.

The ESAComp software provides user-friendly tools to introduce geometrical imperfections into the geometry. The shape of the imperfection can be generated with a linear buckling analysis and scaled by a user-defined amplitude. For cylindrical shells the distorted shape can be based on analytical formulas as well. ESAComp acts as an efficient tool for studying the imperfection sensitivity through the alternation of the shape and amplitude of the imperfection, and thus helps in finding a robust design in the preliminary design phase.

References

[1] *ESAComp - Software for Analysis and Design of Composites*, Release 4.5.2, ESAComp web site. Available at http:// www.esacomp.com.

[2] *Elmer Models Manual*, CSC – IT Center for Science, December 21, 2015, Elmer web site https://www.csc.fi/web/elmer.

[3] T. von Kármán, H. S. Tsien, The Buckling of Thin Cylindrical Shells under Axial Compression, *Journal of the Aeronautical Sciences*, 8:303–312, 1941. Reprinted in *Journal of Spacecraft and Rockets*, 40(6):898-907, 2003. doi:10.2514/2.7056.

[4] *Buckling of Thin-walled Circular Cylinders*, NASA SP-8007, NASA Langley Research Center, Hampton, VA, United States, 1 August 1968.

[5] E. Riks, The Application of Newton's Method to The Problem of Elastic Stability, *Journal of Applied Mechanics*, 39:1060–1065, 1972. doi:10.1115/1.3422829.

[6] E. Ramm, Strategies for Tracing the Nonlinear Response Near Limit Points, *Nonlinear Finite Element Analysis in structural Mechanics*, Springer Verlag, Bochum, 1981.

[7] T. J. R. Hughes, F. Brezzi, On drilling degrees of freedom, *Computer Methods in Applied Mechanics and Engineering*, 72:105–121, 1989. doi:10.1016/0045-7825(89)90124-2.

[8] F. Brezzi, M. Fortin, R. Stenberg, Error analysis of mixed-interpolated elements for Reissner-Mindlin plates, *Math. Models Methods Appl. Sci.*, 1:125–151, 1991.

[9] R. Kouhia, On the Solution of Non-linear Finite Element Equations, *Computers and Structures*, 44:243–254, 1992. doi:10.1016/0045-7949(92)90243-S.

[10] M. Lyly, R. Stenberg, T. Vihinen, A stable bilinear element for the Reissner-Mindlin plate model, *Computer Methods in Applied Mechanics and Engineering*, 110.3:343–357, 1993. doi:10.1016/0045-7825(93)90214-I

[11] H. P. Fuchs and M. W. Hyer The Nonlinear Prebuckling Response of Short Thin-Walled Laminated Composite Cylinders in Bending, *Composite Structures*, 35(3):309–324, 1996. doi:10.1016/0263-8223(95)00152-2.

[12] R. Rolfes, K. Rohwer, Improved transverse shear stresses in composite finite elements based on first order shear deformation theory, *International Journal for Numerical Methods in Engineering*, 40:51–60, 1997. doi:10.1002/(SICI)1097-0207(19970115)40:1<51::AID-NME49>3.0.CO;2-3.

[13] C. Bisagni, Numerical Analysis and Experimental Correlation of Composite Shell Buckling and Postbuckling, *Composites: Part B*, 31:655–667, 2000. doi:10.1016/S1359-8368(00)00031-7.

[14] M. Lyly, On the connection between some linear triangular Reissner-Mindlin plate bending elements, *Numerische Mathematik*, 85:77–107, 2000. doi:10.1007/s002110050478.

[15] H.-R. Meyer-Piening, M. Farshad, B. Geier, R. Zimmerman, Buckling Loads of CFRP Composite Cylinders under Combined Axial and Torsion Loading - Experiments and Computations, *Composite Structures*, 53:427–435, 2001. doi:10.1016/S0263-8223(01)00053-8.

[16] J. N. Reddy, Mechanics of Laminated Composite Plates and Shells - Theory and Analysis, CRC Press, Florida, 2004.

[17] C. Hühne, *Robuster Entwurf beulgefährdeter, unversteifter Kreiszylinderschalen aus Faserverbundwerkstoff*, PhD Thesis, Braunschweig Technical University, Germany, 2005.

[18] C. Hühne, R. Rolfes, J. Tessmer, A new approach for robust design of composite cylindrical shells under axial compression, *Proc. 9th European Conference on Spacecraft Structures, Materials and Mechanical Testing*, 10-12 May, 2005, Noordwijk, The Netherlands, ESA SP-581, 2005.

[19] P. Kere, M. Lyly, On Post-Buckling Analysis and Experimental Correlation of Cylindrical Composite Shells with Reissner-Mindlin-Von Kármán Type Facet Model, *Computers & Structures*, 86:1006–1013, 2008. doi:10.1016/j.compstruc.2007.04.025.

[20] *Space Engineering, Buckling of Structures*, ECSS-E-HB-32-24A, ESA-ESTEC, Noordwijk, The Netherlands, 24 March 2010.

[21] P. Kere, M. Lyly, Reissner-Mindlin-Von Kármán Type Shell Facet Model for Buckling Simulation of Imperfect Cylindrical Composite Shells, *Mechanics of Advanced Materials and Structures*, 18:115–124, 2011. doi:10.1080/15376494.2010.496063.

[22] *Proc. of the 12th European Conference on Spacecraft Structures, Materials & Environmental Testing*, 20-23 March, 2012, Noordwijk, The Netherlands, ESA SP-691, 2012.

[23] P. Kere, Design with Composites, *Encyclopedia of Composites*, pp. 725–737, Wiley & Sons, Inc., 2012.

Harri Katajisto
Componeering Inc.
Itämerenkatu 8, FI-00180 Helsinki
harri.katajisto@componeering.com

Petri Kere
KONE Corporation
P.O. Box 677, FI-05801 Hyvinkää
petri.kere@kone.com

Mikko Lyly
ABB Oy
P.O. Box 186, FI-00381 Helsinki
mikko.lyly@fi.abb.com